ELSEVIER

Journal of Nuclear Materials 306 (2002) 44–53

journal of nuclear materials

www.elsevier.com/locate/jnucmat

Oxidation characteristics of basal (0 0 0 2) plane and prism (1 1 $\bar{2}$ 0) plane in HCP Zr

Hyun Gil Kim [a], To Hoon Kim [a], Yong Hwan Jeong [b,*]

[a] Department of Materials Science and Engineering, Yonsei University, Sinchon-dong 134, Seodaemoon-ku, Seoul 120-749, South Korea
[b] Zirconium Fuel Cladding Team, Korea Atomic Energy Research Institute, P.O. Box 105, 305-600 Yusong, Daejon, South Korea

Received 11 January 2002; accepted 5 August 2002

Abstract

The oxidation characteristics of (0 0 0 2) basal plane and (1 1 $\bar{2}$ 0) prismatic plane of an unalloyed Zr were investigated. From the Zr crystal bar, the specimen representing a single crystal was prepared to be coarse enough to have its grain be $4 \times 4 \times 1$ mm^3 in size. After identifying the crystallographic orientations and planes by X-ray diffraction (XRD), the samples were cut out in such a way as the cutting planes could correspond to the desired crystallographic planes. Oxidation tests were carried out in water at 360 °C. The oxidation rate of the (1 1 $\bar{2}$ 0) prismatic plane was faster than that of the (0 0 0 2) basal plane. The analysis of oxide using the synchrotron XRD revealed that the oxide grown at the basal plane had the preferred (2 0 0) plane in mono-ZrO_2, while the oxide at the prismatic plane grew at both the (2 0 0) and (0 0 2) planes of mono-ZrO_2. In addition, the oxide layer that had formed at the basal plane having only one preferred growth plane exhibited a high fraction of columnar oxide and a relatively wide range of protective barrier layer. These results mean that the characteristics of the preferred planes of mono-ZrO_2 play an important role on the oxidation rate of Zr single crystal.
© 2002 Elsevier Science B.V. All rights reserved.

1. Introduction

Much work has been carried out on the crystal characteristics formed on pure Zr to investigate the oxidation behavior of Zr alloy. Especially, Ploc and co-workers [1–5] concentrated on the crystallographic orientation relationship between Zr matrix and oxide during oxidation process. In their studies, the epitaxial layer of $ZrO_2 < 200$ nm in thickness was extensively examined by transmission electron microscopy (TEM); the epitaxy of ZrO_2 on the (0 0 0 1) plane in α-Zr [1,3], the characteristics of oxide film on Zircaloy-2 [2], the epitaxy of ZrO_2 on the (1 1 $\bar{2}$ 0) plane in α-Zr [4] and (1 0 $\bar{1}$ 0) plane in α-Zr [5]. However, the relationship between epitaxial oxide layer and oxidation rate pf Zr was not well explained.

On the other hand, Wilson [6] reported that the (1 0 $\bar{1}$ 1) and (1 1 $\bar{2}$ 0) planes in α-Zr matrix showed lower oxidation rate than (0 0 0 1) and (1 0 $\bar{1}$ 0) planes when the spherical single crystal specimen was tested at 360 °C in air for 1.5 h. Wanklyn [7] also reported that the oxidation rate of the crystallographic plane in the specimen decreased in the order of (1 0 $\bar{1}$ 2), (1 1 $\bar{2}$ 0), (1 0 $\bar{1}$ 0), (1 0 $\bar{1}$ 1) and (0 0 0 2) plane when the polycrystalline Zr having different orientations was tested at 500 °C in steam for 40 min. It was also reported Pemsler [8] that the oxidation rate of polycrystalline Zr was reduced to the minimum when the *c*-axis was normal to the surface plane but it became maximum when the *c*-axis was inclined to the surface plane of the specimen by 20°.

In addition, Bibb and Fascia [9] observed the epitaxial relationship of (0 0 0 1)‖(1 $\bar{1}$ 1) between Zr matrix and the monoclinic oxide layer. The oxidation was

* Corresponding author. Tel.: +82-42 868 2322; fax: +82-42 862 0432.
E-mail address: yhjeong@kaeri.re.kr (Y.H. Jeong).

0022-3115/02/$ - see front matter © 2002 Elsevier Science B.V. All rights reserved.
PII: S0022-3115(02)01226-6

accelerated on the (0 0 0 1) plane at post transition in the single crystal of pure Zr. Charquet et al. [10] argued that the texture formation on the (0 0 0 2) plane parallel with the surface of polycrystalline Zr specimen resulted in better corrosion resistance. According to Li et al.'s study [11] on the anisotropy of oxygen diffusion in the HCP structure, the oxygen diffusion rates along the [0 0 0 1] and $[1 0 \bar{1} 0]$ directions in the pure Zr are almost the same even though this result is still controversial. As described above, the results of the previous studies on the relationship between the oxidation behavior and the crystallography of the HCP structure of Zr were inconsistent and limited for the full understanding of the oxidation characteristics of pure Zr. For the effective design of the advanced Zr alloys having the improved oxidation resistance, it is essential to fully understand the oxidation characteristics of Zr matrix.

In this study, the oxidation characteristics at the (0 0 0 2) basal plane and the $(1 1 \bar{2} 0)$ prismatic plane of a pure Zr single crystal were investigated to elucidate the effect of the crystallography of the HCP structure on the oxidation characteristics of pure Zr. The oxide formed on the specimen with different crystallographic orientation was characterized using TEM, synchrotron X-ray diffraction (XRD) method and electrochemical impedance spectroscopy. The oxide growth mechanism was discussed in a viewpoint of the relationship of Zr matrix orientation and oxide crystal structure at transition point.

2. Experimental procedures

A high purity Zr having the coarse grain of ~5 mm was provided by WahChang in the form of a crystal bar and its chemical composition is shown in Table 1. The square plates of $4 \times 4 \times 1$ mm^3 were prepared by cutting the bar. A lot of cuttings were tried to get the suitable specimens having only one grain that is made of a single crystal. The crystallographic orientation of the single crystal plates was determined by the θ–2θ method using the XRD, and then the plates having the (0 0 0 2) basal plane and $(1 1 \bar{2} 0)$ prism plane were selected as the specimens. In the θ–2θ method, the angle (2θ) between the X-ray ring and the detector was maintained constant while the location of the sample represented by θ was varied. After mechanical polishing, oxidation tests were carried out in a 18.9 MPa static autoclave at 360 °C. Oxidation behavior was evaluated by measuring the oxide thickness of the specimen at the pre-determined time interval using SEM. The characteristics of the oxide layer were examined by using XRD, TEM, and impedance on the oxide layer with the same thickness. Particularly, the synchrotron X-ray (Line 3C2) at Po-hang Accelerator Laboratory in Korea was employed to analyze the preferred orientation of oxide growth on the planes of (0 0 0 2) and $(1 1 \bar{2} 0)$. Jeong et al. [12] reported that the Synchrotron X-ray scattering was more an accurate technique to detect the crystallography of thin oxide film than the conventional low angle XRD. For the synchrotron X-ray analysis, the θ–2θ method was also used. The phases that had formed at the interface between the oxide layer and matrix were identified by the low angle XRD. For the low angle XRD analysis, the incident beam angle was 2° and 2θ was varied in the range of 20–40°. TEM examination was conducted on the ion-milled samples by using JEOL 2000FX2. The impedance was measured using K0235 flat cell (EG & G PAR). For the measurement of the electro-chemical impedance, IM5D spectroscopy (Zahaner in Germany) was used under the conditions of 100 mHz–2 MHz and in 0.05 M H_2SO_4 medium at room temperature. Before the electro-chemical impedance measurement, the specimens were soaked in the medium for 10 h to fill the cracks and pores fully with the medium.

Table 1
Impurity analysis of zirconium crystal bar

Element	Results	Element	Results
Al	<20	Nb	<50
B	0.3	Ni	<35
C	24	O	<50
Cd	<0.25	P	<3
Co	<10	Pb	<25
Cr	<50	Si	<10
Cu	<10	Sn	<10
Fe	258	Ta	<50
H	18	Ti	<30
Hf	32	U	<1.0
Mn	<25	V	<25
Mo	<10	W	<25
N	<20	–	–

3. Results and discussion

3.1. Crystallography of the sample

Fig. 1 shows the optical microstructures and the XRD profiles of the small specimens used for this study. In the optical microstructures, the grain boundaries were not observed. This means that specimens were prepared to have a single crystal. Instead of boundaries, many twins were observed in the matrix. This type of twins would be formed during the manufacturing of the crystal bar Zr in WahChang. In order to confirm the single crystal Zr, XRDs were performed on all the tested samples. As shown in Fig. 1(a) and (b), the XRD scanning from 20° to 60° revealed one peak at 34.84° of 2θ corresponding to (0 0 0 2) plane and another peak at 56.94° of 2θ corresponding to $(1 1 \bar{2} 0)$ plane, respectively. It was confirmed

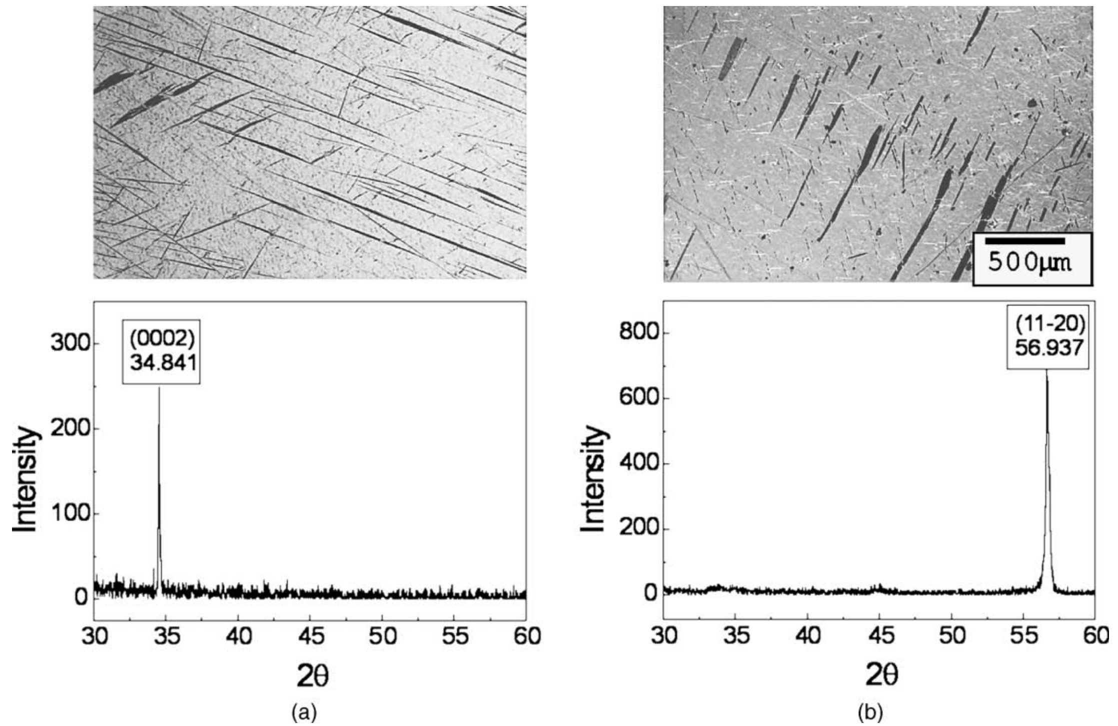

Fig. 1. Optical microstructures and X-ray spectra of zirconium crystal bar; (a) basal plane (0 0 0 2) and (b) prism plane (1 1 $\bar{2}$ 0).

from XRD analysis that the specimens from the coarse grain crystal bar Zr represented the single crystal. Also, the specimens observed by TEM for analyzing the precipitates, but the precipitates did not observed in grain of the specimens. It was thought that the precipitates formed at grain boundary and did not effect on the oxidation of specimens having different planes.

3.2. Oxidation behavior

Fig. 2 shows the oxide thickness observed by SEM. The oxide layer has different thickness by the plans at same oxidation time and it is not observed the protrude that refers by Wanklyn [7]. As shown in SEM micrographs of Fig. 2, the specimen having (0 0 0 2) plane showed thin oxide, while the one having (1 1 $\bar{2}$ 0) plane very thick oxide. It is considered from the this result that the oxidation rate mainly depend on the crystal plane even though a little effect of specimen edge may affect to the overall oxidation rate of small specimens. The variation of oxide thickness was plotted as a function of exposure time in Fig. 3. In the basal (0 0 0 2) plane, the oxide thickness of the specimens increased up to about 1.3 μm during a time of 40 h and then saturated without

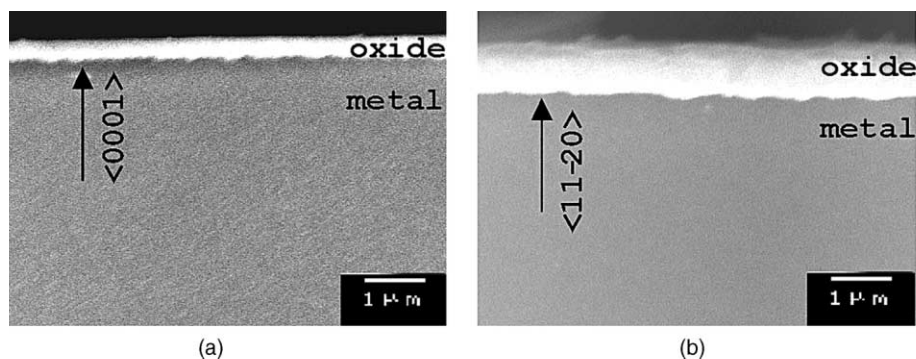

Fig. 2. SEM micrographs of oxide thickness of crystal Zr bar sample formed at 360 °C for 5 h; (a) basal plane (0 0 0 2) and (b) prism plane (1 1 $\bar{2}$ 0).

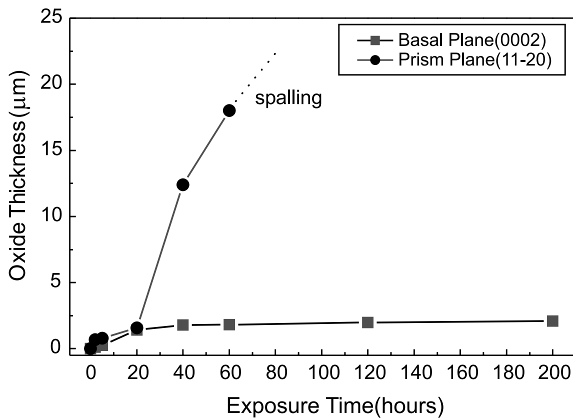

Fig. 3. Corrosion behaviors of zirconium crystal bar in water at 360 °C.

rapid acceleration. However, in the prismatic $(1 1 \bar{2} 0)$ plane, the oxide thickness had rapidly increased after 20 h. This trend on the oxidation kinetics in the crystallographic plane is consistent with the experimental results reported by Pemsler [8] and Charquet et al. [10], but is inconsistent with that by Wilson [6] and Wanklyn [7]. A close inspection of the oxidation behavior revealed that, even though the overall oxidation rate was higher in the $(1 1 \bar{2} 0)$ plane than the (0 0 0 2) plane, the oxidation rate on the $(1 1 \bar{2} 0)$ plane at the initial stage to 20 h was faster than that on the (0 0 0 2) plane. This result can be explained in the viewpoint of oxygen diffusion rate as shown in Fig. 4. The oxygen atoms in the specimen having (0 0 0 2) plane can diffuse through the close packed basal plane, while the oxygen atoms in the specimen having $(1 1 \bar{2} 0)$ plane diffuse through the non-close packed prismatic plane. The oxygen diffusion rate primarily depends on the planar atomic density of the diffusion plane. In addition, the oxygen diffusion path would be symmetric at an equal distance on the basal plane but it would be asymmetric on the prismatic plane.

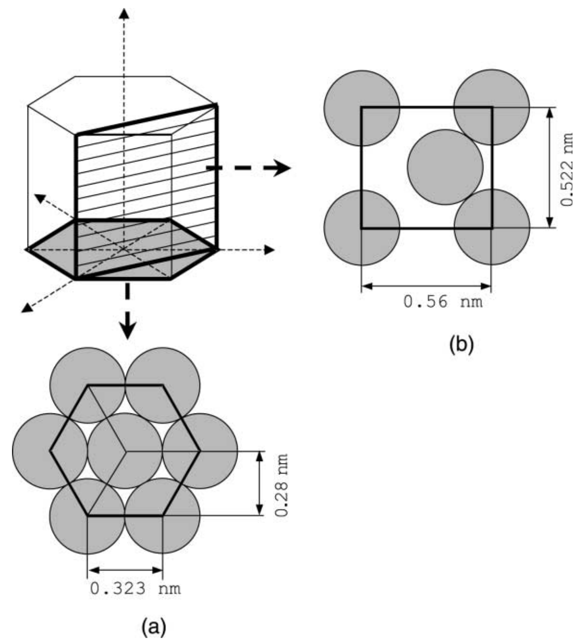

Fig. 4. Schematic diagram of hexagonal planes in α zirconium; (a) basal plane (0 0 0 2) and (b) prism plane $(1 1 \bar{2} 0)$.

These findings strongly indicate that the planar atomic density and atom array of the plane play a critical role on the oxidation kinetics over the oxide thickness about 1 μm.

Fig. 5 shows the oxide morphology in the metal/oxide interface of corroded specimens for 20 h. The oxide thickness of two samples is similar from the Fig. 1, but the oxide morphology is quite different depending on the crystal plane. The oxide formed in (0 0 0 2) plane shows the small lump shape while the oxide formed in $(1 1 \bar{2} 0)$ plane the coarse lump shape. This different oxide morphology may be caused by the different oxidation characteristics in each plane of matrix. The twins in the

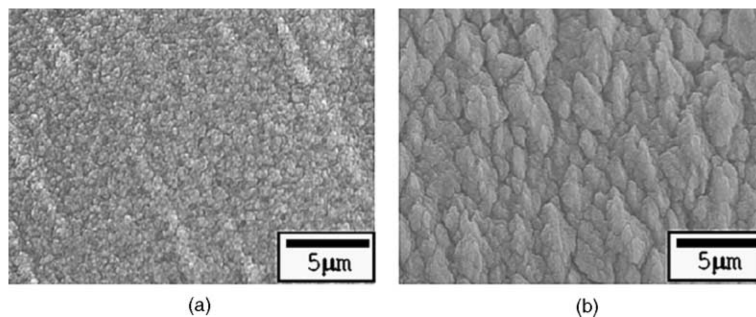

Fig. 5. SEM oxide morphologies of metal–oxide interface of crystal Zr bar sample formed at 360 °C for 20 h; (a) oxide morphology formed on basal plane (0 0 0 2) and (b) oxide morphology formed on prism plane $(1 1 \bar{2} 0)$.

matrix can affect on the oxidation rate. However the twin effect can be excluded in the oxidation behaviors of two different the comparison of plane because the shapes and morphologies of twin were very similar in both specimens as shown in Fig. 1.

3.3. Characteristics of oxide layer

3.3.1. XRD analysis

In order to identify the crystal structures of oxides formed on the basal and prismatic planes, the synchrotron X-ray analysis was carried out on the samples having the same oxide thickness (1.3 μm) and the result is shown in Fig. 6. In the oxide layer formed on the basal plane, the (2 0 0) monoclinic peak was dominantly observed with a minor portion of (0 0 2) and ($\bar{1}$ 1 1) peak. In the oxide layer formed on the prismatic plane, in addition to the (2 0 0) monoclinic peak, the (0 0 2) monoclinic peak developed well while ($\bar{1}$ 1 1) monoclinic peak still remained as a small peak. It was found from the synchrotron X-ray analysis that the preferred growth plane in the monoclinic ZrO_2 formed on the basal plane was the (2 0 0) plane. While (2 0 0) or (0 0 2) plane could be a preferred growth plane in the monoclinic ZrO_2 formed on the prism plane by increasing the oxide thickness. The peaks representing the tetragonal phase were not detected due to the absence of factors stabilizing the tetragonal ZrO_2. The result of low angle XRD analysis in Fig. 7 is similar to that of the synchrotron X-ray analysis in Fig. 6. However, it is of interest to note the presence of the peak for the (1 1 1) plane of monoclinic ZrO_2. Generally, the low angle XRD analysis provides more information on the oxide/metal interface than high angle method, which had been used in the synchrotron X-ray analysis. It indicated that the crystal structure of the oxide at the interface was more complex than that expected. The relatively wide spreading of the peaks resulted from the high strain state in the vicinity of the interface. As similar to the synchrotron X-ray analysis, the peak for the (1 1 1) planes of tetragonal ZrO_2 that is known to have a protective property was not detected. It

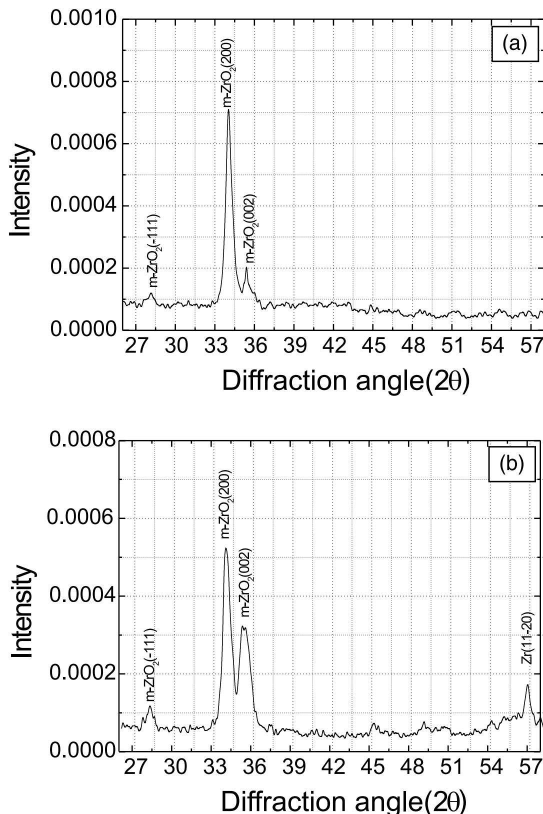

Fig. 6. Synchrotron X-ray scattering on the oxides having equal thickness (1.3 μm); (a) oxide formed on basal plane (0 0 0 2) and (b) oxide formed on prism plane (1 1 $\bar{2}$ 0).

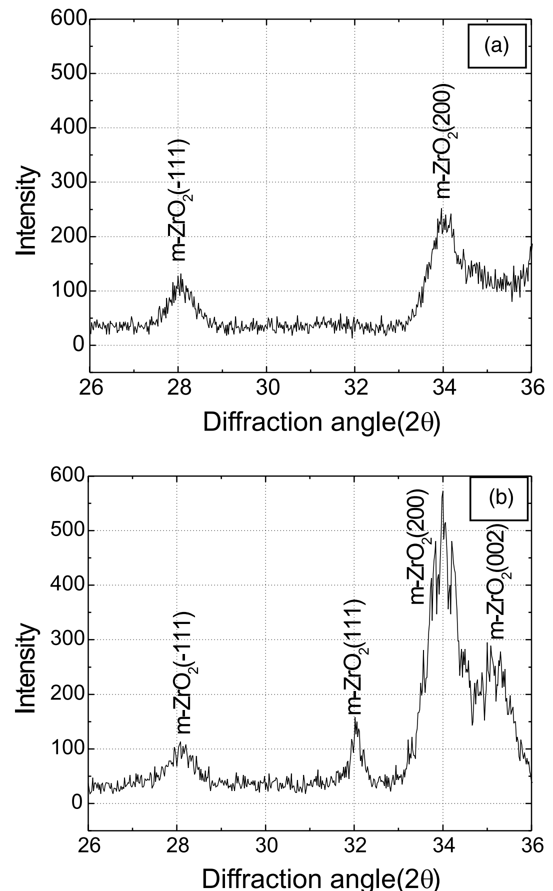

Fig. 7. Low-angle XRD spectra on the oxides at metal–oxide interface having equal thickness (1.3 μm); (a) oxide formed on basal plane (0 0 0 2) and (b) oxide formed on prism plane (1 1 $\bar{2}$ 0).

is equal to the results of Ploc [5] and Bibb and Fascia [9]. The absence of tetragonal ZrO_2 would result from a fast corrosion rate in this specimen compared to the commercial Zr alloys. From the two kinds of XRD analysis on the thin oxide, it is suggested that the oxidation characteristics of pure Zr would be controlled by the preferred growth of monoclinic ZrO_2.

A schematic illustration for the growth mechanism of the monoclinic ZrO_2 oxide layer is shown in Fig. 8. Fig. 8(a) and (b) describe the crystal structure of monoclinic ZrO_2 and the crystallographic relationship between the oxide layer and the matrix, respectively. In Fig. 8(b), the symbols of square, rectangle and parallelogram represent the (2 0 0), ($\bar{1}$ 1 1) and (0 0 2) planes of monoclinic ZrO_2, respectively. It is worth mentioning that the shape of the projection of the planes with respect to their growth direction matches with each symbol: i.e., the (2 0 0) plane grows along the ⟨1 0 0⟩ direction; the ($\bar{1}$ 1 1) plane grows along the ⟨$\bar{1}$ 1 1⟩ direction; the (0 0 2) plane grows along the ⟨0 0 1⟩ direction. As seen in Fig. 8(b), the majority of the oxide formed on the basal plane consisted of the (2 0 0) plane of monoclinic ZrO_2. For the prismatic plane, even though the (2 0 0) plane of monoclinic ZrO_2 would help cause the majority of the oxide, the (0 0 2) plane would also contributes to a considerable portion of the oxide. If the oxide was grown with a multi-variant, the mismatches between oxides having different directions would have occurred inevitably, and they would play a role in the effective path for oxygen diffusion. Accordingly, it was thought that the oxidation rate on the prismatic plane containing more mismatches was enhanced compared to that on the basal plane.

3.3.2. TEM analysis

One of the effective methods to investigate the relationship between corrosion and the characteristics of the oxide layer is the microstructure study of oxide by using TEM [13–15]. TEM micrographs in the oxide formed on the basal and prismatic planes are shown in Fig. 9(a) and (b), respectively.

The equiaxed oxide structures were observed in the outside of oxide while columnar oxide structures were observed in the vicinity of the oxide–metal interface. However, the oxide formed on the prismatic plane contained more equiaxed structures and less columnar

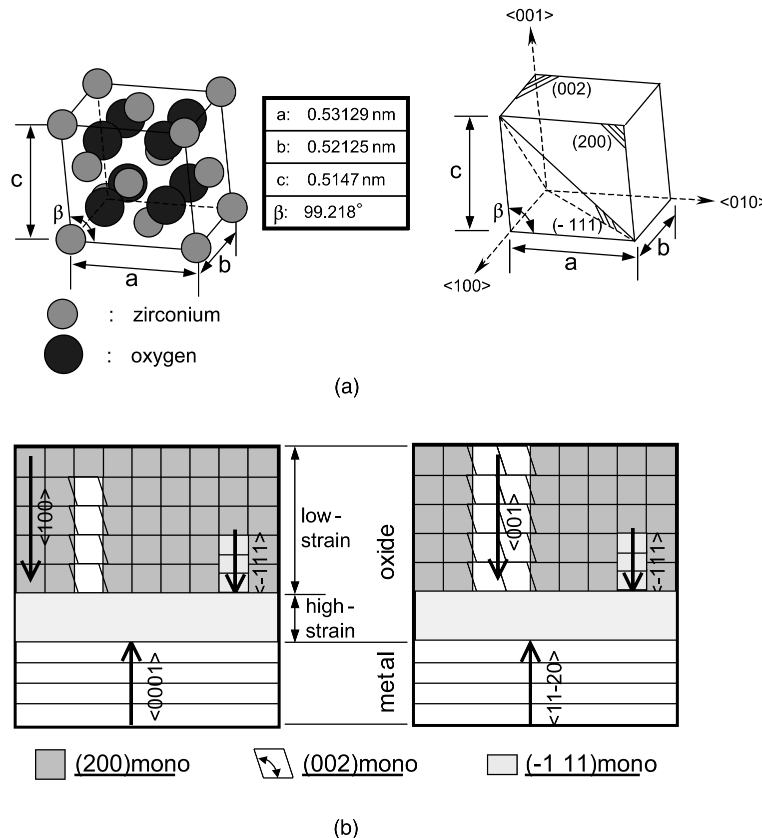

Fig. 8. Schematic model of oxide crystal structure on the zirconium crystal plane; (a) crystal structure of monoclinic ZrO_2 and (b) crystal relation of oxide and metal.

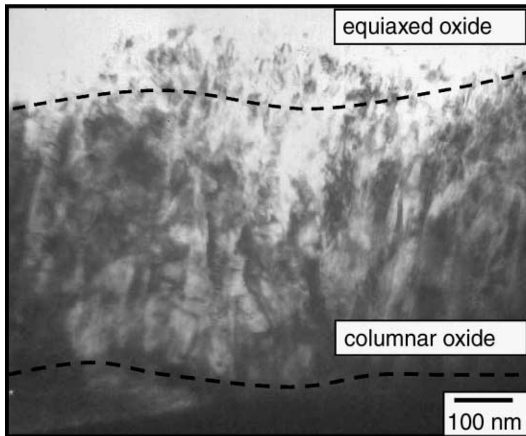

(a)

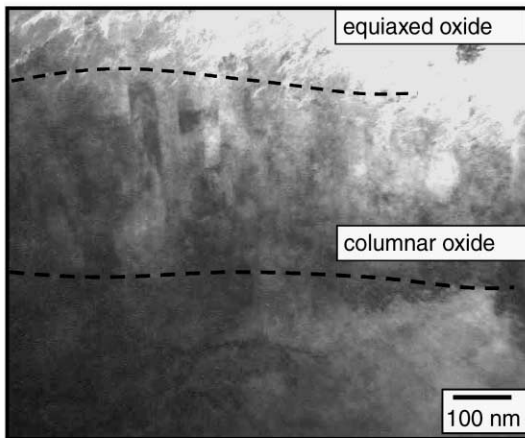

(b)

Fig. 9. Cross-sectional TEM micrographs of zirconium–oxide formed in pre-transition; (a) basal plane (0 0 0 2) and (b) prism plane (1 1 $\bar{2}$ 0).

structures than that formed on the basal plane. Some columnar oxides on the prismatic plane were not well defined showing a short length. This means that the columnar structure is being transformed to the equiaxed structure. The preferred growth of (2 0 0) plane in the monoclinic ZrO_2 is effective to maintain the stable columnar microstructure. If the oxide formed in the prismatic plane contains a more equiaxed structure, the corrosion rate of the prismatic plane will be accelerated due to the high fraction of grain boundary area serving the effective oxygen path.

3.3.3. Electro-chemical impedance spectroscopy (EIS) analysis

Generally, the impedance at a high frequency range is associated with the characteristics of the oxide formed at

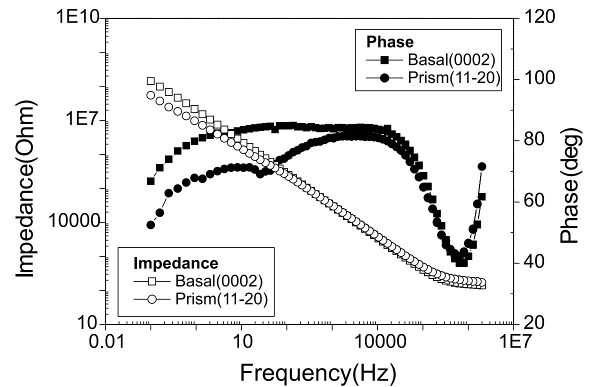

Fig. 10. Bode plots for the oxides formed at pre-transition regime with the different crystal planes.

the initial stage and that at a low frequency ranges it is associated with the characteristics of the protective oxide layer at the interface [16–18]. The Bode plot of EIS in the corrosion samples is shown in Fig. 10. The slope in the oxide formed on the basal plane was about −1 and the phase angle at a high frequency range was close to 90°. This type of the oxide layer is known to be a corrosion-resistant characteristic due to the good capacitance and the formation of the space charge layer at the oxide surface. For the oxide layer formed on the prismatic plane, the slope and phase angle at a low frequency range were lower showing the two peaks than those in the basal plane. However, at the high frequency, the slope was close to −1. This means that the oxide formed on the prismatic plane consists of two different layers.

In Fig. 11, the schematic plot of the double oxide layer and the corresponding equivalent circuit is constructed to illustrate the EIS result for the oxide layer formed on the prismatic plane. The EIS behavior of TiO_2 and Al_2O_3 layers has been well described by the model in Fig. 11 [19,20]. By applying this model, the capacitance and resistance of the inner and outer layers can be obtained by comparing the experimental EIS results with the equivalent circuit. In addition, it is possible to estimate the inner layer thickness from the capacitance. For the ideal parallel capacitor, the impedance can be described in terms of the thickness by Barberis and Frichet [21]

$$Z = t/2\pi f \varepsilon\varepsilon_0 A, \tag{1}$$

where f is the frequency, A is the surface area, ε_0 is the absolute dielectric constant (8.86×10^{-12} F/m) and ε is the relative dielectric constant of ZrO_2. For capacitance, $Z = 1/2\pi fC$. Therefore, the capacitance thickness is expressed by

$$t = \varepsilon\varepsilon_0 A/C, \tag{2}$$

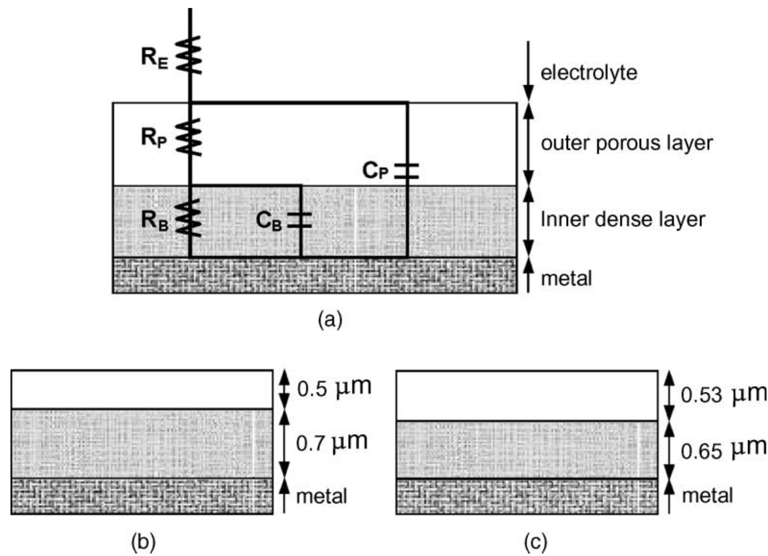

Fig. 11. Schematic drawings of oxide microstructures at pre-transition regime by EIS; (a) equivalent circuit, (b) basal plane (0 0 0 2) and (c) prism plane (1 1 $\bar{2}$ 0).

t is in mm and C is in μF/cm^2. Since t is inversely proportional to the capacitance as in Eq. (2), the layer thickness can be estimated from the layer capacitance. The capacitance of the inner non-penetrable layer is obtainable by analyzing the EIS spectrum and the components of the equivalent circuit. Usually, μ in Eq. (2) is 13–22. If the values for the inner and outer layers are measured precisely, the oxide layer thickness and the corrosion resistance of the sample in the autoclave can be easily obtained. The calculated characteristics of the oxide layer are listed in Table 2. The subscripts p and b denote the outer porous layer and the inner non-penetrable layer, respectively. Tt is the calculated total thickness of the layer predicted from Eqs. (1) and (2) and Tm is the total thickness estimated from the weigh gain. The Tt for the layer formed on the basal plane is very close to Tm within the experimental error. The R is resistance for the layer formed on the basal and prismatic plane, the porous layer has similar constant on the planes but the dense layer has higher value on the basal plane. However, a significant error occurred between Tt and Tm for the layer formed on the prismatic plane. This error resulted from the fact that Eq. (2) is not valid for the porous layer as shown in Fig. 9.

On the oxide growth mechanism, the oxide structure was composed of the multi-layer in a viewpoint of the microstructure or crystal structure [22,23]. The schematic plot for the oxidation behavior on the basal and the prismatic planes was constructed in Fig. 12. At the initial stage, the oxidation was dominated by matrix

Table 2
Electrochemical properties of oxide layer

Oxide type	Items	Value	t (μm)[a]	Tt (μm)[b]	Tm (μm)[c] (W.G.)
Basal (0 0 0 2)	RE (Ω)	110.8			
	R_p (kΩ)	996.3			
	R_B (MΩ)	393.3			
	C_P (nF)	4.486	0.5	1.3	1.3
	C_B (nF)	3.144	0.7		
Prism (1 1 $\bar{2}$ 0)	R_E (Ω)	143.7			
	R_P (kΩ)	823.9			
	R_B (MΩ)	78.27			
	C_P (nF)	4.191	0.53	1.18	1.3
	C_B (nF)	3.43	0.65		

[a] Porous and barrier oxide thickness obtained by impedance.
[b] Total oxide thickness obtained by impedance.
[c] Total oxide thickness obtained by weight gain.

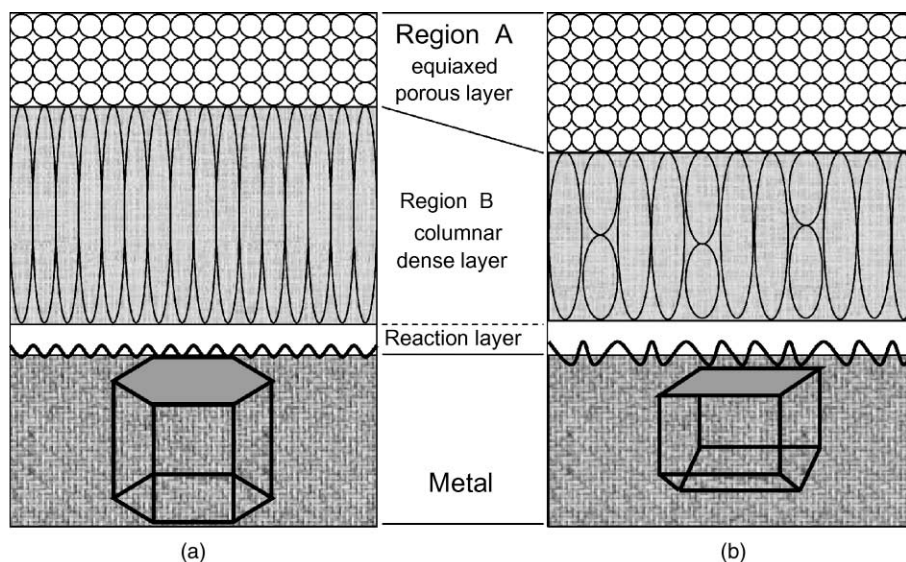

Fig. 12. Schematic drawings of oxide microstructures formed at pre-transition regime with different crystal planes; (a) basal plane (0 0 0 2) and (b) prism plane (1 1 $\bar{2}$ 0).

crystallography. On the prismatic plane, a relatively wide equiaxed oxide is formed compared to the basal plane due to faster oxygen diffusion. Then, the oxidation rate becomes slow. In initial state, the oxidation behavior differ by reporter, it would be the difference of preparing method of specimen and oxidation condition. In Region B, the oxidation is rate-controlled by oxygen diffusion and the matrix crystallography. In addition, the columnar oxides are formed along the oxygen diffusion direction. The crystal structure of the columnar oxide is affected by the characteristics of the oxide formed at the initial stage and matrix crystallography. At the metal–oxide interface the oxide formed new nucleus having high strain, and then the oxide formed the columnar by re-orientation that would be caused by varying the strain state as away from the matrix. It may be caused the orientation of oxide crystal structure by matrix characteristics. The columnar oxide formed on the prismatic plane is wide and discrete due to the multi-variant growth, as described in Fig. 7. In addition, The EIS results characterizing the capacitance and resistance of the oxide layer revealed that the corrosion resistance of the oxide layer formed on the basal plane was superior to that of the oxide layer formed on the prismatic plane.

4. Conclusions

In the present investigation, the oxidation characteristics at the (0 0 0 2) basal plane and the (1 1 $\bar{2}$ 0) prismatic plane of a pure Zr single crystal were investigated. The oxidation rate on the prismatic plane was faster than that on the basal plane. The faster oxidation rate on the prismatic plane is attributed to the fact that the two or more preferred oxide growth planes, (2 0 0) and (0 0 2), operated in the oxide formed on the prismatic plane while only one preferred oxide growth plane, (2 0 0), was active in the oxide formed on the basal plane. The oxide layer formed at the basal plane having only one preferred growth plane contained a large fraction of columnar oxide and a relatively wide protective barrier layer. The corrosion resistant columnar oxide was stabilized when the (2 0 0) plane of the monoclinic ZrO_2 became the preferred growth plane. In summary, the oxidation behavior of pure Zr primarily depends on the preferred growth plane of the monoclinic ZrO_2 consisting the oxide layer.

Acknowledgement

This project has been carried out under the Nuclear Fuel R&D program by KAERI.

References

[1] R.A. Ploc, J. Nucl. Mater. 28 (1968) 48.
[2] R.A. Ploc, M.A. Miller, J. Nucl. Mater. 64 (1977) 71.
[3] R.A. Ploc, J. Nucl. Mater. 110 (1982) 59.
[4] R.A. Ploc, J. Nucl. Mater. 113 (1983) 74.
[5] R.A. Ploc, J. Nucl. Mater. 115 (1983) 110.
[6] J.C. Wilson, Trans. AIME 197, 284 (1953) 182.

[7] J.N. Wanklyn, ASTM 368 (Special Publication) (1964) 368.
[8] J.P. Pemsler, J. Electrochem. Soc. 105 (1958) 315.
[9] A.E. Bibb, J.R. Fascia, Trans. Metal Soc. AIME 230 (1964) 415.
[10] D. Charquet, R. Tricot, J.-F. Wadier, ASTM STP 1023 (1989) 374.
[11] Bing Li, A.R. Allnatt, C.-S. Zhang, P.R. Norton, Surf. Sci. 330 (1995) 276.
[12] Y.H. Jeong, J.H. Baek, S.J. Kim, H.G. Kim, H. Ruhmann, J. Nucl. Mater. 270 (1999) 322.
[13] F. Garzarolli, H. Seidel, R. Tricot, J.P. Gros, ASTM STP 1132 (1991) 395.
[14] H. Anada, K. Takeda, ASTM STP 1295 (1996) 35.
[15] Y.H. Jeong, H.G. Kim, T.H. Kim, J. Nucl. Mater. (submitted for publication).
[16] J.A. Grandle, S.R. Taylor, Corrosion 50 (10) (1994) 792.
[17] F. Mansfeld, M.W. Kendig, Corrosion 41 (8) (1985) 490.
[18] D.F. Wei, I. Chatterjee, D.A. Jones, Corrosion 51 (2) (1995) 97.
[19] J. Pan, D. Thierry, C. Leygraf, Electrochem. Acta 41 (1996) 1143.
[20] A. Baltat-Baaia, N. Celati, M. Keddam, H. Takenouti, R. Wiart, Mater. Sci. Forum 111 (1992) 359.
[21] P. Barberis, A. Frichet, J. Nucl. Mater. 273 (1999) 182.
[22] C. Roy, G. David, J. Nucl. Mater. 37 (1970) 71.
[23] R.A. Ploc, J. Nucl. Mater. 61 (1976) 79.